

1 **Photodynamic priming mitigates chemotherapeutic selection pressures and** 2 **improves drug delivery**

3 **Authors:** Huang-Chiao Huang^{1,2†}, Imran Rizvi^{1,2†}, Joyce Liu^{1,2†}, Sriram Anbil^{1,2,3}, Ashish
4 Kalra⁴, Helen Lee⁴, Yan Baglo^{1,2}, Nancy Paz⁴, Douglas Hayden⁵, Steve Pereira⁶, Brian W.
5 Pogue⁷, Jonathan Fitzgerald⁴, Tayyaba Hasan^{1,2,8*}

6 ¹Wellman Center for Photomedicine, Massachusetts General Hospital and Harvard Medical
7 School, Boston, MA 02114, USA.

8 ²Department of Dermatology, Massachusetts General Hospital, Boston, MA 02114, USA.

9 ³The University of Texas School of Medicine at San Antonio, San Antonio, TX 78229, USA.

10 ⁴Merrimack Pharmaceuticals, Inc., Cambridge, MA 02139, USA.

11 ⁵MGH Biostatistics Center, Massachusetts General Hospital, Boston, MA 02114, USA.

12 ⁶UCL Institute for Liver and Digestive Health, University College London, London NW3 2QG,
13 UK.

14 ⁷Thayer School of Engineering, Dartmouth College, Hanover, NH 03755, USA.

15 ⁸Division of Health Sciences and Technology, Harvard University and Massachusetts Institute of
16 Technology, Cambridge, MA 02139, USA.

17 *To whom correspondence should be addressed: Tayyaba Hasan, Ph.D.; Professor of
18 Dermatology; Professor of Health Sciences and Technology (Harvard-MIT); Wellman Center for
19 Photomedicine, Massachusetts General Hospital, Harvard Medical School; Address: 40 Blossom
20 Street, Bartlett 314, Boston, MA 02114; Phone: 617-726-6996; Email: thasan@mgh.harvard.edu.

21 †These authors contributed equally to this work.

22 **Running title:** PDP overcomes chemotherapeutic selection of stemness markers

23 **Keywords:** Biophysical priming modality, Nanoliposomal irinotecan (ONIVYDE), Combined

24 modality therapy, Pancreatic ductal adenocarcinoma, Tumor permeability

25 **Abstract**

26 Physiological barriers to drug delivery and selection for drug resistance limit survival outcomes
27 in cancer patients. In this study, we present preclinical evidence that a subtumoricidal
28 photodynamic priming (PDP) strategy can relieve drug delivery barriers in the tumor
29 microenvironment to safely widen the therapeutic window of a nanoformulated cytotoxic drug.
30 In orthotopic xenograft models of pancreatic cancer, combining PDP with nanoliposomal
31 irinotecan (nal-IRI) prevented tumor relapse, reduce metastasis and increase both progression-
32 free survival and 1-year disease-free survival. PDP enabled these durable improvements by
33 targeting multiple tumor compartments to (1) increase intratumoral drug accumulation by >10-
34 fold, (2) increase the duration of drug exposure above a critical therapeutic threshold, and (3)
35 attenuate surges in CD44 and CXCR4 expression which mediate chemoresistance often observed
36 after multi-cycle chemotherapy. Overall, our results offer preclinical proof of concept for the
37 effectiveness of PDP to minimize risks of tumor relapse, progression and drug resistance and to
38 extend patient survival.

39

40 **Introduction**

41 Cancer is a constantly evolving disease that relies on both microenvironmental and
42 molecular compartments to resist and adapt to therapeutic insults(1). Significant efforts have been
43 invested in developing chemotherapeutics, biological agents, and cocktails to overcome resistance
44 mechanisms and escape pathways(2,3). However, these intense multimodal regimens have largely
45 been hindered by poor drug penetration into solid tumors(4), transient responses that fail to
46 eradicate aggressive populations with distinct molecular features(5), and significant off-target
47 toxicities associated with anti-cancer agents(6).

48 Here, we report a subtumoricidal photochemistry-based approach (hereafter referred to as
49 Photodynamic Priming, PDP) that primes multiple tumor compartments to enable more potent
50 and sustained anti-tumor activity of the FDA-approved nanoliposomal irinotecan (nal-IRI, also
51 known as MM-398, PEP02, BAX2398)(7). This unique photoinitiated approach offers multiple
52 advantages (**Fig.1**): (i) At the tumor microenvironmental level, PDP enables spatiotemporally
53 controlled targeting of physiological barriers to drug delivery for enhanced therapeutic agent
54 accessibility; (ii) At the molecular level, PDP overcomes chemotherapy-induced enrichment of
55 stemness markers to suppress aggressive tumor relapse; and (iii) PDP's subtumoricidal nature,
56 distinct mechanism of action, and non-overlapping toxicities, enhance chemotherapeutic efficacy
57 with no additional side effects *in vivo*. We provide evidence that a clinically feasible PDP
58 regimen realizes these complementary interactions to significantly potentiate the efficacy of
59 multi-cycle nal-IRI, resulting in prolonged local tumor control, reduced metastatic burden, and
60 enhanced survival outcomes *in vivo* in two mouse models of human pancreatic ductal
61 adenocarcinoma (PDAC).

62 PDAC is a devastating disease characterized by a dense fibrous stroma, that impedes drug
63 delivery, and by a profound resistance to standard chemotherapy(8). Therapeutic strategies
64 designed to ablate this tumor-associated desmoplasia yielded disappointing clinical results(9,10),
65 in part because PDAC-stroma interactions are extraordinarily complex and incompletely
66 understood(11). In 2015, nal-IRI combined with 5-fluorouracil and leucovorin was approved to
67 treat gemcitabine-refractory metastatic PDAC(12). Developed by Drummond and colleagues,
68 nal-IRI improves the circulation half-life, pharmacokinetics and intratumoral accumulation of
69 irinotecan and its active metabolite, SN-38, while minimizing toxic side effects(13). The superior
70 *in vivo* anti-cancer activity of nal-IRI, as compared to free irinotecan, is related to nal-IRI's
71 ability to extend the duration of intratumoral SN-38 above a critical threshold concentration.(14)
72 However, the high degree of variability in nal-IRI tumor deposition *in vivo* remains a challenge,
73 presumably due to the low permeability of liposomes within some tumors, as described
74 previously(14). Moreover, because PDAC cells are highly resistant to standard chemotherapy(8),
75 it is increasingly evident that intensive chemotherapeutic regimens based on the maximum
76 tolerated dose can impose selection pressures that reveal residual populations of intrinsic or
77 acquired resistant clones, portending a poor outcome(15,16). Prime examples of highly
78 aggressive PDAC subpopulations include cells that overexpress hyaluronan receptor (CD44) and
79 C-X-C chemokine receptor type 4 (CXCR4)(17-19). These markers play pivotal roles in self-
80 renewal, multi-lineage differentiation, chemoresistance, potent proliferative and metastatic
81 capacity of PDAC, and correlate with poor prognosis in patients(17-19). Previous studies have
82 shown that the front-line chemotherapy for PDAC, gemcitabine, induces a significant increase in
83 CD44 (17.5-fold) and CXCR4 (20-fold) protein levels in PDAC cell lines(16,20), and enriches
84 CD44+ cell population by ~40% in patient-derived xenografts and patient samples of PDAC(21).

85 Preventing the selection of these aggressive phenotypes while maintaining cytotoxic efficacy
86 have become highly desirable attributes of any therapeutic regimen. Here, we demonstrate for
87 the first time that PDP simultaneously increases the local nal-IRI concentration in tumors (by
88 enhancing tumor permeability transiently), and attenuates the upregulation of CD44 and CXCR4
89 markers in nal-IRI treated tumors *in vivo*, leading to superior treatment outcomes in orthotopic
90 models of PDAC.

91 PDP is based on the hypothesis that spatiotemporal control of photosensitizer activation
92 can induce enhanced tumor permeability secondary to singlet oxygen generation in the tumor
93 vasculature, stroma, and parenchyma. In addition, because PDP is comprised of subtumoricidal
94 photodynamic therapy (PDT)(22), it has the added advantage of directly activating cancer
95 apoptosis in such a way that bypasses multiple cell death signaling pathways that are typically
96 required by conventional chemotherapy regimens to be effective. Kessel *et al.* first reported that
97 PDT directly induces photodamage to the mitochondria-associated Bcl-2 protein (a major anti-
98 apoptotic factor and mediator of drug resistance) to release mitochondrial cytochrome c (a potent
99 pro-apoptotic signal), thereby initiating apoptosis(23). This direct pathway to cell death suggests
100 that PDT, with sufficient co-localization of photosensitizer and light, is effective even against
101 chemoresistant populations characterized by defective signaling pathways, and thus may prevent
102 enrichment of these specific aggressive subpopulations and their associated molecular
103 characteristics. Building on the recent clinical advances using PDT for locally advanced PDAC
104 patients(24), our findings offer prospects to design new PDP-based approaches that offer dual
105 advantages stemming from enhanced drug accessibility while minimizing treatment-induced
106 molecular selective pressures for long-term anti-tumor efficacy, without additional side effects.

107

108 **Materials & Methods**

109 ***Nanoliposomal BPD (nal-BPD) and nanoliposomal irinotecan (nal-IRI) preparation.***

110 Nanoliposomal benzoporphyrin derivative (nal-BPD) were prepared *via* freeze-thaw
111 extrusion technique as previously described(25). Briefly, dipalmitoylphosphatidylcholine
112 (DPPC), cholesterol, distearoylphosphatidylethanolamine-methoxy polyethylene glycol (DSPE-
113 PEG), and dioleoyltrimethylammoniumpropane (DOTAP) (Avanti Polar Lipids) were mixed in
114 chloroform at 20:10:1:2.5 molar ratio. Two hundred micromolars of BPD (U.S. Pharmacopeial
115 Convention) was dissolved with lipids at a drug-to-lipid ratio of 0.6 mol%. Chloroform was
116 removed by rotary evaporation overnight to afford a thin lipid film. The resulting lipid film was
117 rehydrated with 1mL of phosphate-buffered saline at 45°C, and then subjected to freeze-thaw
118 cycles (4–45°C) for 2 hours. The dispersion was then extruded ten times through 0.1µm
119 polycarbonate membranes at 42°C using a mini-extruder system to form unilamellar vesicles.
120 Un-encapsulated BPD photosensitizers were removed by dialysis (MWCO 300kD) against
121 phosphate-buffered saline. The resulting nal-BPD preparations displayed a particle size of
122 135nm (Polydispersity index ~0.04) and a photosensitizer loading of 3µg BPD/mmol
123 phospholipid. Stability, shelf-life, singlet oxygen yield, photobleaching, quenching, drug release,
124 *in vivo* pharmacokinetics and biodistribution of nal-BPD were previously reported(25). The
125 clinically approved nanoliposomal irinotecan (nal-IRI) and DiIC18(5)-DS dye-conjugated nal-
126 IRI (DiI5-nal-IRI) were kindly provided by Merrimack Pharmaceuticals(13).

127 ***Cell Culture.***

128 Human PDAC cancer cell lines, MIA PaCa-2 and AsPC-1, were purchased from ATCC.
129 All cells were authenticated prior to receipt and were propagated for less than four months after

130 resuscitation. Cultures were tested for mycoplasma as previously described(25). All cell lines
131 were cultured in humidified CO₂ atmosphere at 37°C using media recommended by the vendor.

132 ***Orthotopic mouse model and treatments.***

133 All treatment and care of animals were in accordance with the protocol approved by
134 Massachusetts General Hospital (MGH) Institutional Animal Care and Use Committee
135 (IACUC). MIA PaCa-2 or AsPC-1 cells were implanted orthotopically in 4-6 weeks old male
136 Swiss nude mice (20-25g) to establish xenograft tumors. Animals were anesthetized with
137 100mg/kg ketamine and 10mg/kg xylazine, and a small left abdominal flank incision was made
138 to exteriorize the pancreas. Subsequently, a suspension of 1x10⁶ cancer cells in 25µL of chilled
139 culture media mixed with an equal volume of chilled Matrigel[®] was injected into the mouse
140 pancreas, and the incision was sutured aseptically. Treatments were initiated nine days after
141 cancer cell implantation when tumor volumes reached approximately 50mm³—determined by
142 ultrasound imaging (Vevo LAZR; VisualSonics) as previously described(25). Injections of nal-
143 BPD and nal-IRI (20mg/kg, hydrochloride salt) for treatment were done intravenously (tail vein)
144 in 200µL sterile phosphate-buffered saline. Mice were randomized into groups that received (i)
145 no-treatment, (ii) photodynamic priming (PDP), (iii) nal-IRI (four cycles on days 9, 12, 17, and
146 21 after tumor implantation), (iv) single cycle nal-IRI (sc-nal-IRI; one cycle on day 9 after tumor
147 implantation) (v) PDP+sc-nal-IRI, (vi) PDP+nal-IRI. For sub-tumoricidal PDP, orthotopic
148 tumors were surgically exposed (as for tumor implantation) at one hour after intravenous
149 injection of nal-BPD (0.25mg/kg BPD equivalent). Tumors of mice receiving nal-BPD were
150 irradiated with NIR light using a 690nm diode laser (High Power Devices), delivered at an
151 irradiance of 100mW/cm² to achieve a fluence of 75J/cm². Following PDP, the incisions were
152 closed with 4-0 Ethilon sutures and the animals were allowed to recover. Tumor growth in every

153 animal was longitudinally monitored every 3-5 days using non-invasive ultrasound imaging as
154 described previously. At each time point, tumor volume was calculated using hemiellipsoid
155 formula ($\pi \cdot L \cdot W \cdot H / 6$, where L, W and H, are the tumor length, width and height), which was
156 validated against the three-dimensional volume reconstruction algorithm of the Vevo2100
157 software(25). To calculate the specific growth rate (SGR) of tumor, the following formula was
158 used: $SGR = (1/V)(dV/dt)$, where V is tumor volume and t is time. Change in mouse body weight
159 was monitored before tumor implantation and longitudinally after treatment as a metric of
160 systemic toxicity. For survival studies, moribundity was used as the endpoint with proper
161 justification and special approval by MGH IACUC. Progression-free survival (PFS) is
162 defined as the time from treatment initiation to any increase in tumor volume or death from any
163 cause.

164 *Pharmacokinetic studies.*

165 When the average tumor volume reached approximately 50 mm^3 , mice were randomized
166 into groups that received (i) no-treatment, (ii) PDP, (iii) single cycle of nal-IRI at 20mg/kg (sc-
167 nal-IRI; on day 9 after tumor implantation), and (iv) PDP+sc-nal-IRI. At 1, 4, 24, 72, 168 hours
168 after treatment, mice were euthanized by CO_2 asphyxiation followed by blood collection, and
169 then mice were perfused with phosphate-buffered saline prior to harvesting tumor and other
170 normal tissues. Bloods samples were collected in tubes containing lithium heparin and were
171 centrifuged to separate the plasma immediately after sample collection. All samples were stored
172 at -80°C until analyses. Tumor and plasma were analyzed for irinotecan and SN-38
173 concentrations using the HPLC method previously described(14). Briefly, tumors were weighed
174 and homogenized for 2 minutes in 20% w/v water using a TissueLyser (Qiagen). The
175 homogenates were extracted by mixing 0.1mL homogenate with 0.9mL 1% acetic acid/methanol

176 followed by 10s vortexing and placing at -80°C for 1 hour. The samples were centrifuged at
177 10,000rpm for 10 minutes at room temperature and supernatants collected for HPLC analysis
178 (Dionex). The samples and standards (irinotecan and SN-38) were analyzed using a C18 reverse
179 phase column (Synergi Polar-RP 80A 250 \times 4.60 mm 4 μm column). The drug metabolites were
180 eluted running a gradient from 30% acetonitrile; 70% 0.1% TFA/H₂O to 68% acetonitrile; 32%
181 0.1% TFA/H₂O during a 13 minutes span at a flow rate of 1.0mL/min. The initial elute
182 composition was restored after 14 minutes and continued for 6 minutes before the next injection.
183 The irinotecan peak was detected at \sim 7.7 minutes and the SN-38 peak eluted at \sim 8.4 minutes,
184 using an in-line fluorescence detector excited at 372nm and emitting at 556nm.

185 ***Tumor vasculature and Dil5-nal-IRI fluorescence imaging.***

186 Tumor-bearing mice were randomized into groups that receive (i) no-treatment, (ii) nal-
187 BPD, (iii) PDP, (iv) Dil5-nal-IRI, and (v) PDP + Dil5-nal-IRI. At 4, 24, 72 hours after treatment,
188 mice were intravenous (tail vein) injected with 100 μL of Fluorescein-labeled *Lycopersicon*
189 *esculentum* (tomato) lectin (1mg/mL in phosphate-buffered saline, Vector Laboratories) to label
190 the vascular endothelium. At 5 minutes after tomato-lectin intravenous injection, mice were
191 euthanized by CO₂ asphyxiation followed by perfusion with phosphate-buffered saline prior to
192 harvesting tumors. Excised tissues were embedded in optimal cutting temperature compound and
193 frozen at -80°C . A cryotome was used to cut 20- μm -thick cryosections. Sections were mounted
194 (Invitrogen SlowFade Gold with 4',6-diamidino-2-phenylindole, DAPI) with a coverslip and
195 sealed with nail polish for confocal fluorescence imaging (Olympus FluoView 1,000 confocal
196 microscope) using a 10x0.4 numerical aperture (NA) or a 20x0.75 NA objective. Excitation of
197 DAPI, tomato-lectin labeled vasculature, and DiIC18(5)-DS dye conjugated nal-IRI (Dil5-nal-
198 IRI) was carried out using 405, 488, and 635-nm lasers, respectively, with appropriate filters.

199 ***Immunofluorescence imaging of CD44 and CXCR4 markers.***

200 Treatment impacts on the tumoral expression of CD44, and CXCR4 were investigated.
201 Briefly, orthotopic pancreatic tumors were excised on 60 and 120 days after tumor implantation
202 (*i.e.* 51 and 111 days after treatment initiation), embedded in optimal cutting temperature
203 compound and frozen at -80 °C. A cryotome was used to cut 20- μ m-thick cryosections. Sections
204 were (i) fixed in ice-cold 1:1 acetone:methanol for 10 min, (ii) air dried for 30 minutes, and (iii)
205 washed three times in phosphate-buffered saline. A blocking solution (Dako Protein Block
206 Reagent) was applied for 30 min followed by application of the immunostains, at ~5 μ g/mL
207 monoclonal antibody (MAb) each diluted in background reducing Dako Antibody Diluent for
208 overnight at 4°C in a humidifying chamber. Finally, the slides were washed again three times,
209 mounted (Invitrogen SlowFade Gold with 4',6-diamidino-2- phenylindole, DAPI) with a
210 coverslip and sealed with nail polish. Confocal fluorescence imaging was performed using an
211 Olympus FluoView 1,000 confocal microscope with a 10x0.4 numerical aperture (NA) or a 20x
212 0.75NA objective. Excitation of DAPI, anti-human cytokeratin 8 (clone LP3 K IC3165G; R&D
213 Systems) MAb-Alexa Fluor 488 conjugates, and anti-human CD44 (clone DB105; Miltenyi
214 Biotec) MAb- APC-Vio770™ conjugates was carried out using 405-, 405-, and 635-nm lasers,
215 respectively, with appropriate filters. At least 10 images, evenly distributed across the entire
216 tumor cross-section, were collected from 3 tumor samples for each condition.

217 ***Western Blot.***

218 Protein expression was analyzed using a standard Western protocol (Bio-Rad). As briefly
219 described, tissue lysates (10 μ g) were separated on 10% precast polyacrylamide gel (Mini-
220 PROTEAN TGX, Bio-Rad) and transferred onto PVDF membrane (Thermo). Subsequent to
221 blocking with 5% milk/TBST solution, proteins were further detected using antibodies against

222 CD44 (1:1000, Santa Cruz sc7946), CXCR4 (1:500, Abcam ab93478), and E-Cadherin (1:500,
223 Abcam ab15148). Anti GADPH antibodies (1:5000, Cell Signaling 2118S) were used for loading
224 control. Visualization of protein bands was developed by chemiluminescence (ECL, Bio-Rad)
225 with exposure to X-ray film (Thermo). The quantitative analysis of protein expression was done
226 using ImageJ software. Western blot analyses of target proteins were repeated at least for three
227 times.

228 ***Measurement of metastatic burden.***

229 A quantitative reverse transcription-polymerase chain reaction (qRT-PCR) assay was
230 performed on excised liver, lung, diaphragm, and paraaortic lymph nodes to estimate the number
231 of human cancer cells in excised organs as described and validated previously(26). Briefly, qRT-
232 PCR is used to measure the total number of human cancer cells from the level of human and
233 mouse glyceraldehyde 3-phosphate dehydrogenase (GAPDH) housekeeping genes. The entire
234 freshly excised liver, lung, diaphragm, paraaortic lymph nodes were collected at the treatment
235 endpoint and snap frozen in liquid nitrogen. The frozen samples were then pulverized and
236 homogenized in TRIzol solution, followed by RNA extraction (RNAeasy Plus Mini Kit;
237 Qiagen). Human and mouse GAPDH gene were measured using custom synthesized primers
238 (Invitrogen). For each specimen, the cycle threshold (Ct) from human GAPDH gene was
239 quantified into *number of cancer cells* using a standard curve generated with a set of organ
240 lysates from no-tumor control mice mixed with different numbers of human cancer cells.

241 ***Statistical analyses.***

242 Results are mean \pm standard error of the mean (SEM). Statistical tests were carried out
243 using GraphPad Prism (GraphPad Software). Specific tests are indicated in the figure captions.
244 All reported P values are two-tailed. *In vivo* results and fluorescence intensity analyses were

245 analyzed using nonparametric tests (the Bonferroni-corrected Mann-Whitney U test or Kruskal–
246 Wallis one-way ANOVA with appropriate post hoc test); the D’Agostino & Pearson omnibus
247 normality test ($\alpha=0.05$; requires $n \geq 8$ replicates per group to perform testing) identified
248 deviations from normality within these data sets. One-way ANOVA was applied to test for
249 longitudinal treatment interactions, based on the linearized slope of each tumor volume growth
250 curve. Log-transformation was applied to linearize the tumor volume growth curve for each
251 animal. No exclusion criteria were used, and no data points or animals were excluded from
252 analysis. Two-way ANOVA was also applied to test for synergistic treatment interactions, using
253 the slope of each tumor volume growth curve; log-transformation was applied to linearize the
254 tumor volume growth curve for each animal. No exclusion criteria were used, and no data points
255 or animals were excluded from analysis. Survival curves were created using the method of
256 Kaplan and Meier. The log-rank test was used to test if the difference between survival times
257 between two groups is statistically significant or not. Investigators were blinded to experimental
258 groups during tumor volume monitoring and survival studies unless noted otherwise.
259

260 **Results**

261 *PDP induces physiological changes in vascular permeability to enhance the tumor*
262 *pharmacokinetics of nal-IRI.*

263 To evaluate PDP-mediated changes in tumor vascular permeability, DiIC18(5)-DS dye-
264 conjugated nal-IRI (DiI5-nal-IRI) was administered by intravenous injection in mice bearing
265 orthotopic MIA PaCa-2 tumors (50mm³). Confocal imaging showed PDP enhanced DiI5-nal-IRI
266 extravasation and accumulation in tumors at 4 hours after DiI5-nal-IRI injection (**Fig.2A**).

267 Without PDP, only a small amount of DiI5-nal-IRI extravasated along the immediate vicinity of
268 tumor blood vessels at an average distribution area of 0.002mm² at 4 hours after injection. In
269 contrast, PDP significantly broadened the intratumoral dissemination of DiI5-nal-IRI along the
270 periphery of blood vessels by 100 times to 0.22±0.02mm² ($P<0.001$; **Fig.2B**). Furthermore, DiI5-
271 nal-IRI was highly retained in PDP-treated tumors for at least 24-hours (**Fig.2C**). The ratio of the
272 fluorescence signal intensities (FSI) of accumulated DiI5-nal-IRI at 4 and 24 hours after injection
273 was found to be 6.2 and 10-fold higher in the PDP-treated tumors, respectively (**Fig.2C**;
274 $P<0.001$), compared to the control tumors using the following equation: $(FSI_{PDP+DiI5-nal-IRI}-FSI_{no-}$
275 $treatment)/(FSI_{DiI5-nal-IRI}-FSI_{no-treatment})$.

276 Irinotecan is a camptothecin prodrug that is converted by carboxylesterases to produce
277 the active SN-38 (7-ethyl-10-hydroxycamptothecin) metabolite, which is approximately 100 to
278 1000-fold more potent(27). The tumoral irinotecan and SN-38 pharmacokinetic profiles of nal-
279 IRI were evaluated with and without PDP (**Fig.2D,E**). In the orthotopic MIA PaCa-2 model,
280 intravenous administration of a single cycle of nal-IRI (20mg/kg irinotecan hydrochloride salt)
281 resulted in 0.35%ID/g (1390ng/g) of tumoral irinotecan 24 hours after injection (**Fig.2D**). In
282 contrast, following PDP+nal-IRI, intratumoral irinotecan levels were 11-fold higher (3.5%ID/g)

283 and remained above 1%ID/g for 72 hours (**Fig.2D**). Similarly, SN-38 cleared earlier from the
284 tumors following nal-IRI injection to 12.8ng/g (32.6nM) within 24 hours, while ‘PDP+nal-IRI’
285 treated tumors exhibited a high intratumoral SN-38 level of above 50ng/g (127.4nM) for up to
286 72-hours following treatment (**Fig.2E**). PDP did not alter tumor carboxylesterase activity
287 (**Fig.2F**), as a result the time-dependent change in the molar ratio of irinotecan-to-SN-38 in
288 tumors treated with nal-IRI was similar to the ‘PDP+nal-IRI’ group (**Fig.2G**).

289 ***PDP of local tumors followed by multi-cycle nal-IRI prevents rapid tumor regrowth and***
290 ***synergistically enhances long-term tumor growth inhibition.***

291 To assess the efficacy of PDP and nal-IRI in controlling localized tumors *in vivo*,
292 treatments were performed nine days following orthotopic implantation of MIA PaCa-2 or
293 AsPC-1 human PDAC cells in mice, when tumors reached approximately 50mm³ in volume. The
294 following treatments were randomly administered to mice: (i) no-treatment; (ii) PDP; (iii) nal-
295 IRI; and (iv) PDP+nal-IRI (**Fig.3A**). For PDP, light (690nm) irradiation was performed one hour
296 after a single intravenous injection of a nanoliposomal formulation of the photosensitizer,
297 benzoporphyrin derivative (nal-BPD at 0.25mg/kg), to induce sub-tumoricidal tumor
298 permeabilization. The 1-hour photosensitizer-light interval was used to achieve a balanced
299 distribution of nal-BPD in both the tumor vasculature and parenchyma, based on our previous
300 experience(28). Four intravenous injections of nal-IRI were administered over two weeks, and
301 each injection contained 20mg/kg irinotecan hydrochloride salt. Tumor growths were
302 longitudinally monitored using non-invasive ultrasound imaging. In MIA PaCa-2 tumors
303 (derived from a primary tumor), both ‘PDP+nal-IRI’ and ‘nal-IRI’ exhibited a significant
304 inhibition of tumor growth during the treatment period, whereas, continued tumor growth was
305 observed in ‘no-treatment’ and ‘PDP’ over this same period (**Fig.3B-D**). At 30 days post-

306 implantation, the mean tumor volume reduction in mice treated with ‘nal-IRI’ and ‘PDP+nal-
307 IRI’ was 89% and 96%, respectively, compared to ‘no-treatment’ animals (**Fig.3C**). However,
308 shortly after termination of treatment and up to 120 days following implantation, animals treated
309 with ‘nal-IRI’ experienced a rapid tumor regrowth at a specific growth rate (SGR) of
310 $4.8\pm 0.3\%/day$, which is significantly higher than the $2.6\pm 0.2\%/day$ SGR in ‘no-treatment’
311 ($P<0.05$; **Fig.3E**). In contrast, ‘PDP+nal-IRI’ not only significantly inhibited tumor volume
312 growth by 96% by day 32 (with a SGR of $-4.7\pm 1\%/day$) (**Fig.3D**), but also continued to suppress
313 tumor growth at an SGR of $1.7\pm 0.9\%/day$ for a prolonged period of up to 120 days (**Fig.3E**). The
314 effect of ‘PDP+nal-IRI’ on tumor growth inhibition was found to be highly synergistic compared
315 to monotherapies ($P=0.0041$; **Fig.S1**). Furthermore, mouse body weight was longitudinally
316 monitored before and after treatment as a metric of toxicity (**Fig.S2**). In ‘PDP+nal-IRI’ animals,
317 the change in mouse weight was consistent with ‘nal-IRI’ mice, indicating that PDP does not
318 appreciably add to the *in vivo* systemic toxicity. The gain in mouse weight after single cycle nal-
319 IRI was comparable to the combination of PDP and a single cycle nal-IR, whereas, a transient
320 loss in mouse weight up to 8% was observed following four cycles of nal-IRI treatment both in
321 presence and absence of PDP. These observations suggest that the sub-tumoricidal PDP
322 approach does not further increase the systemic toxicity of nal-IRI in mice. The long-term
323 efficacy of ‘PDP+nal-IRI’ was also evaluated in a model for more aggressive PDAC using
324 AsPC-1 cells derived from a metastatic lesion (**Fig.3F-I**). In agreement with the literature, AsPC-
325 1 tumors in ‘no-treatment’ controls exhibit a significantly higher tumor SGR ($10.9\pm 0.4\%/day$),
326 compared to MIA PaCa-2 tumors ($6.7\pm 0.7\%/day$) ($P=0.0025$). Both ‘nal-IRI’ and ‘PDP+nal-IRI’
327 significantly reduced AsPC-1 tumor volume growth for at least 30 days, but did not completely
328 arrest tumor growth (**Fig.3E-G**). However, between days 30 and 120, AsPC-1 tumors that

329 received ‘PDP+nal-IRI’ exhibited a much lower regrowth rate ($3.7\pm 0.7\%$ /day), compared to ‘no-
330 treatment’ ($\sim 6\%$ /day) ($P < 0.05$; **Fig.3H**). Ultimately, combining PDP with nal-IRI resulted in
331 superior AsPC-1 volume control compared to the nal-IRI treated tumors at day 120 ($P < 0.05$;
332 **Fig.3D**).

333 ***PDP overcomes chemotherapeutic selection pressures that cause upregulation of cancer stem***
334 ***cell markers and dedifferentiation.***

335 To assess whether the rapid MIA PaCa-2 tumor regrowth following four cycles of nal-IRI
336 observed in figure 3B occurred as a result of chemotherapeutic selection pressures, we assessed
337 the expression of CD44, CXCR4, and E-Cadherin, which are associated with tumor progression,
338 stemness and differentiation. Tumors were harvested at days 60 and 120 following implantation
339 because they approximated the time-points of significant post-treatment tumor regrowth for the
340 ‘nal-IRI’ and ‘PDP+nal-IRI’ groups, respectively (**Fig.3B**). Immunofluorescence imaging
341 (**Fig.4A**) revealed that four cycles of nal-IRI treatment significantly enriched CD44 and CXCR4
342 expression by $\sim 180\%$ compared to the ‘no-treatment’ tumors at day 60 ($P \leq 0.05$; **Fig.4B,C**). In
343 contrast, PDP alone did not promote CD44 and CXCR4 expression of in MIA PaCa-2 tumors.
344 Interestingly, ‘PDP+nal-IRI’ not only significantly reduced the expression of CD44 ($\sim 65\text{-}80\%$
345 reduction; $P \leq 0.01$) compared to the monotherapies, but it also maintained CXCR4 expression at
346 the base line level by day 60. Similarly at day 120, confirmed by western blot (**Fig.4D,E**), the
347 expression of CD44 and CXCR4 were ~ 2 folds higher in the nal-IRI treated tumors compared to
348 the ‘no-treatment’ and ‘PDP alone’ groups. In contrast, ‘PDP+nal-IRI’ was able to maintain
349 CD44 and CXCR4 expressions at a baseline level despite tumor growth after treatment. Tumoral
350 CD44+, CXCR4+, and CD44+/CXCR4+ cell populations were evaluated by
351 immunofluorescence double staining at days 60 day 120 (**Fig.4F**). At day 120 (**Fig.4G**), nal-IRI

352 treatment increased the tumoral CD44+, CXCR4+, and CD44+/CXCR4+ areas by ~1.22, 1.59
353 and 2 folds, respectively, compared to no-treatment tumors. Both ‘PDP’ and ‘PDP+nal-IRI’
354 significantly reduced CD44+, CXCR4+, and CD44+/CXCR4+ cell populated areas by ~43, 71
355 and 90% respectively, compared to ‘nal-IRI’ treated tumors. At day 60, immunoblotting showed
356 that nal-IRI treated tumors exhibited the highest level of E-cadherin expression (**Fig.4H,I**)
357 relative to all other groups. However, at day 120, ‘no-treatment’, ‘PDP’, and ‘nal-IRI’ tumors
358 exhibited a complete loss of E-Cadherin expression, whereas a strong expression of E-Cadherin
359 was observed in the ‘PDP+nal-IRI’ group. These data suggest that at early time points (day 60),
360 with chemotherapy alone there is evidence of E-Cadherin enriched population. However as the
361 disease progresses (day 120) only the combination of PDP and nal-IRI overcomes
362 chemotherapy-induced selection pressures, as evidenced by decreased levels of the stemness
363 markers CD44 and CXCR4 and increased expression of E-Cadherin. To investigate whether this
364 time-dependent shift towards a population distribution with a less stem-like and a more
365 differentiated phenotype may reduce tumor spread and improve outcomes, we evaluated
366 metastases control and long-term (>1 year) survival benefit of ‘PDP+nal-IRI’.

367 ***PDP of primary tumors enhances nal-IRI chemotherapeutic control of metastases.***

368 Locally advanced PDAC often metastasizes to distant organs. Our orthotopic mouse
369 model of PDAC resembles typical clinical patterns of dissemination, displaying (i) extensive
370 primary tumor growth that extends to the stomach and duodenum, (ii) metastatic infiltrates to the
371 liver, and (iii) distant metastases to the retroperitoneal lymph nodes, diaphragm and lung
372 (**Fig.S3**). The impact of combining PDP with four cycles of nal-IRI on metastasis control was
373 evaluated in mice bearing orthotopic MIA PaCa-2 tumors (**Fig.5A**). At day 60, both ‘PDP+nal-
374 IRI’ and ‘nal-IRI’ significantly reduced the liver and distant organ metastatic burden by at least

375 22,000-fold, as compared to the ‘no-treatment’ group (**Fig.5B,C**). Subtumoricidal PDP alone did
376 not significantly reduce the metastatic burden, compared to the ‘no-treatment’ (**Fig.5B,C**). These
377 results suggest that the metastatic disease is primarily and effectively controlled by ‘nal-IRI’ at
378 early time points. At day 60, both ‘nal-IRI’ and ‘PDP+nal-IRI’ completely inhibited liver
379 metastasis and significantly reduced distant organ (lung, diaphragm, lymph node) metastases to
380 less than 50 cancer cells, compared to ‘no-treatment’ mice (>1 million cancer cells at lung,
381 diaphragm, lymph node) (**Fig.5D**). Importantly, the benefit in controlling metastases provided by
382 nal-IRI alone over 60 days was lost by day 120. Only ‘PDP+nal-IRI’ achieved a significant
383 reduction in the overall and distant organ metastases by an average of ~16,000-fold and ~40,000-
384 fold ($P<0.01$), respectively, compared to ‘no-treatment’ (**Fig.5D**). In contrast, metastatic burden
385 in ‘nal-IRI’ group was not significantly different from ‘no-treatment’ mice at day 120 (**Fig.5D**).
386 In addition to metastatic burden, the incidence of metastases in MIA PaCa-2 mouse model was
387 monitored at days 60 and 120. At day 60 (when diaphragm metastases were observed in 100% of
388 animals), ‘PDP+nal-IRI’ significantly reduced the incidence of diaphragm metastases by 66%,
389 while ‘nal-IRI’ did not reduce the incidence of metastasis (**Fig.5E**). Consistent with the
390 metastatic burden data, by day 120, the incidence of liver, lung, and lymph node metastases in
391 the ‘PDP+nal-IRI’ mice was dramatically reduced to 6.7% and 33%, respectively, in contrast to
392 the high incidence of liver and distant metastases (60-100%) for the ‘no-treatment’, ‘PDP’, and
393 ‘nal-IRI’ groups (**Fig.5E**).

394 ***PDP and multi-cycle nal-IRI prolong survival and reduce endpoint disease burden in two***
395 ***PDAC models.***

396 Most patients with PDAC are diagnosed at an advanced stage and rapidly succumb to
397 their disease. It was, therefore, critical to determine if the significant and prolonged improvement

398 in metastasis control provided by ‘PDP+nal-IRI’ translated to durable survival enhancement.
399 Using moribundity as the endpoint (**Fig.6A**), the orthotopic models of MIA PaCa-2 and
400 AsPC-1 cells demonstrated median survival times of 146 days (4.9 months) and 82.5 days
401 (2.75 months), respectively (**Fig.6B-D**). In the MIA PaCa-2 model, sub-tumoricidal PDP
402 combined with four cycles of nal-IRI significantly prolonged the median overall survival
403 (OS) to 280 days (9.3 months), compared to 170 days (5.6 months) with ‘nal-IRI’ (**Fig.6B**;
404 $P<0.01$). All animals in the ‘no-treatment’ and ‘nal-IRI’ groups were dead at days 228 and
405 215, respectively. In the ‘PDP’ group, 92% of the mice died by day 208, while 1 out of 13
406 (8%) survived to day 337. Importantly, 25% of animals in the ‘PDP+nal-IRI’ group survived
407 to day 450 (~1.23 years), when the study was terminated. The pancreas and distant organs in the
408 mice treated with ‘PDP+nal-IRI’ were confirmed to be tumor-free by ultrasound imaging,
409 complete necropsy, and qRT-PCR (see Methods). Combined PDP and multi-cycle nal-IRI
410 doubled the median progression-free survival (PFS) of MIA PaCa-2 tumor-bearing mice to 76
411 days (2.53 months), compared to the PSF of mice treated with ‘nal-IRI’ (35 days) ($P<0.001$;
412 **Fig.6C**). It is noteworthy that although the combination of PDP and a *single cycle* of nal-IRI,
413 synergistically reduced acute tumor burden (**Fig.S1**), no survival benefit was observed (**Fig.S4**).
414 These findings highlight the difficulty in achieving meaningful improvements in treatment
415 response for PDAC and emphasize the need for combination regimens designed to provide
416 durable tumoricidal control. In the AsPC-1 model, combined PDP and four cycles of nal-IRI
417 achieved ~18% tumor-free animal survival and significantly prolonged the median OS of mice to
418 214 days (7.1 months), compared to 82.5 days (~2.75 months) in ‘no-treatment’ mice ($P=0.024$;
419 **Fig.6D**). Although the mice treated with nal-IRI also demonstrated an improved median OS of
420 170 days (5.6 months), it was found to be non-significant ($P=0.3$) compared to the ‘no-

421 treatment' mice. These results, in two animal models, suggest that sub-tumoricidal PDP of
422 primary tumors is crucial to achieving significant and durable survival benefits with nal-IRI. The
423 forest plot (**Fig.6E**) summarizes the hazard ratio data across multiple variables. Here, the
424 hazard ratio is defined as the ratio of the probability of death in the treatment arm to the
425 probability in the no-treatment arm, and represents the instantaneous risk over the study
426 time period. A hazard ratio of less than 0.2 ($P<0.05$) observed in the 'PDP+nal-IRI' group in
427 both MIA PaCa-2 and AsPC-1 models, suggests that animals in 'PDP+nal-IRI' group at any
428 given time point were five times more likely to survive by the next time point compared to the
429 no-treatment group. In contrast, all other treatment groups cross the 1.0 value, indicating the
430 hazard ratio is not significant and there is no clear advantage for 'PDP' and 'nal-IRI' alone
431 compared to the 'no-treatment' arm.

432 We further evaluated the primary tumor weight, ascitic fluid volume, and metastatic
433 burden of animals that reached the moribundity endpoint (excluding tumor-free animals). We
434 observed that 'PDP+nal-IRI' reduced primary tumor weight by 50% in these mice, compared to
435 tumors treated with nal-IRI alone ($P=0.056$; **Fig.6F**). Furthermore, 'nal-IRI' and 'PDP+nal-IRI'
436 significantly reduced the mean ascitic fluid volume to 1.2 ± 0.6 mL ($P\leq 0.05$; **Fig.6G**), compared
437 to the substantial ascitic fluid accumulation (7.6 ± 1.2 mL) observed in the 'no-treatment' and
438 'PDP'. Metastatic burden in mice that reached moribundity was similar in both the 'PDP+nal-
439 IRI' and 'nal-IRI' (**Fig.S5**).

440

441 **Discussion**

442 Nanoliposomal delivery systems offer tools to improve the pharmacokinetic and safety
443 profiles of cytotoxic drugs(29). Nal-IRI, with a favorable irinotecan pharmacokinetic profile, is
444 presently being incorporated into standard treatment paradigms for patients with gemcitabine-
445 refractory metastatic PDAC, due to manageable safety and substantial improvement in survival
446 outcomes(7,12). Previously, we have employed photochemistry to damage multidrug efflux
447 transporter proteins, thereby increasing the intracellular accumulation of nal-IRI in cancer
448 cells.(25) Here, we introduce the concept of subtumoricidal photodynamic priming (PDP) and
449 demonstrate its ability to (i) acutely enhance the intratumoral distribution of nal-IRI by covering
450 100-fold greater portion of the tumor volume, (ii) elevate intratumoral nal-IRI concentrations up
451 to 11-fold at 24 hours after nal-IRI injection, (iii) maintain high intratumoral SN-38
452 concentrations for an extended period of 72 hours. Further investigations into the role of PDP in
453 disrupting and permeabilizing the tumor-associated extracellular matrix are warranted to fully
454 exploit this approach as a tool to modulate primary tumor permeability and enhance cytotoxic
455 drug penetration. Importantly, the spatiotemporal selectivity of PDP—achieved by both passive
456 accumulation of non-toxic photosensitizers and light delivery using optical fiber technology—
457 helped confine this enhanced delivery and pharmacokinetic benefit to the desired disease sites,
458 thereby limiting undesired systemic off-target toxicities. This multi-layered selectivity limits the
459 adverse events typically seen in clinical PDAC to mild abdominal pain, skin irritation, and
460 photosensitivity(24); all of which are non-overlapping with the major side effects of nal-IRI (*e.g.*
461 neutropenia and diarrhea)(7), thus affording a compelling, if often overlooked, rationale to
462 photochemically prime the tumors for nal-IRI. In addition, clinically approved dosing of nal-IRI
463 for PDAC patients is 70 mg/m², and comprises an average of 5.875 cycles (30). In two

464 preclinical *in vivo* orthotopic mouse models, we show that superior outcomes could be achieved
465 with PDP followed by four cycles of nal-IRI at clinically relevant dose of 20 mg/kg (equivalent
466 to human dose ~ 60 mg/m²) over several weeks without compromising nal-IRI efficacy or
467 increasing off-target toxicities. The long-term durability (weeks) of the effect of PDP in
468 enhancing drug delivery is not yet clear, combination of periodic PDP and multi-cycle nal-IRI
469 could potentially further prolong the chemotherapeutic retention in tumors and merits a
470 comprehensive investigation. Furthermore, advances of multi-drug nanoliposomal formulations
471 coupled with targeted co-delivery of photosensitizers and chemotherapeutic agents hold high
472 potential for periodic PDP-based combination therapy to further improve therapeutic outcomes
473 in the future(26,31).

474 Although clinical chemotherapy regimens can appear to be quite effective for advanced
475 PDAC during the treatment period, the use of these intensive treatments at the maximum
476 tolerated dose may allow for the competitive release and unopposed proliferation of resistant
477 cancer cell populations(32,33). In our study, four cycles of nal-IRI effectively arrested local
478 tumor growth and reduced metastatic burden for two months in orthotopic PDAC mouse models.
479 At one month following treatment termination, a rapid aggressive disease relapse occurred in the
480 MIA PaCa-2 model, but not in AsPC-1. This variation in treatment response is not surprising, as
481 the two cells lines are of different origin and characteristics. MIA PaCa-2 cells, are characterized
482 to be CD44+, CD24- and CD133/1-(34,35), and were derived from the pancreas of a patient
483 without prior treatments(36). On the other hand, AsPC-1 cells (CD44+, CD24-)(37) were
484 obtained from the ascites of a metastatic PDAC patient whose disease had already failed both
485 radiation and chemotherapy(36). Not surprisingly these cells express higher levels of CD44(37),
486 greater tumorigenicity and chemoresistance(36,38). While first-line gemcitabine chemotherapy

487 induces up to 20-fold increase in CD44 and CXCR4 expressions in PDAC cell lines(16,20), we
488 showed that the MIA PaCa-2 tumor relapse following multi-cycle nal-IRI treatment was
489 accompanied by 2 folds increase in the tumoral expression of the CD44 and CXCR4 cancer
490 stem-like cell markers. A number of carefully thought-out regimens exploiting the evolutionary
491 dynamics of cancer progression have been proposed for more durable outcomes. Since Fidler and
492 Ellis proposed that “Cancer is a chronic disease and should be treated like other chronic
493 diseases” in 2000(39), new drug administration and therapeutic modalities have been introduced.
494 Most notable amongst these regimens are Hanahan’s “metronomic therapy”(40), Folkman,
495 Kerbel and others studies of using anti-angiogenic therapy to “turn cancer into a manageable
496 chronic disease”(41,42), Gatenby’s “adaptive therapy”(43), as well as the “evolutionary double
497 bind” and “stemming tumor growth” methods(44). However, the actual benefits of these
498 approaches have not yet been confirmed in large-scale clinical trials, presumably because
499 regimens are cumbersome, labor-intensive, and expensive. Here, for the first time, we show that
500 the agnostic nature of PDP modulates all cells alike, mitigating the enrichment of stemness
501 markers (CD44 and CXCR4) and preserving the expression of differentiation markers (E-
502 Cadherin), thereby preventing rapid tumor regrowth and extending the period of tumor growth
503 inhibition. Enrichment in the CD44 and CXCR4 markers represents an unintended “Achilles’
504 heel” for current chemotherapy regimens, and both markers are emerging as potential targets for
505 PDAC treatment(3). The ability of PDP to effectively modulate these markers offers a unique
506 opportunity to potentially alter cancer cell-stromal cell crosstalk, reverse chemoresistance, and
507 inhibit metastases.

508 Clinical studies of treatment failure patterns in PDAC patients have revealed that
509 approximately 30% of patients died with locally destructive disease, whereas 70% died with

510 widespread metastatic disease that most commonly involves the liver in combination with
511 peritoneal and/or lung metastases(45). Systemic nal-IRI chemotherapy appears to be very
512 effective in controlling metastases already, and the PDP approach not only sensitizes primary
513 tumors to nal-IRI for a prolonged acute control, but also further reduced metastatic burden.
514 Typically, tumoricidal photodynamic therapy (PDT) can also elicit distant anti-tumors effects
515 due to the immune stimulation(46), and the fact that our *in vivo* models used in this study were
516 immunocompromised suggests that the indirect metastatic control afforded by sub-tumoricidal
517 PDP is secondary to its ability to simultaneously inhibit CXCR4 expression (a crucial driver for
518 the metastatic phenotype in PDAC) and metastatic escape. Further investigations of PDP in
519 immunocompetent animals to elicit distant anti-tumor immunity are likely to result in superior
520 outcomes that better reflect those that would be seen clinically.

521 Because PDAC is usually diagnosed at an advanced stage and most patients die within
522 two years of diagnosis(47), maximizing quality of life through effective palliative treatments is a
523 critical, and often overlooked, endpoint in preclinical settings(48). The quality of life of the
524 PDAC patient is often impaired by (i) side effects of chemotherapy or pain(49), (ii) extensive
525 primary tumor growth disrupting digestive processes (*e.g.* mass effects affecting the intestines or
526 bile ducts), and (iii) ascites causing abdominal swelling(50). While chemotherapy-induced
527 toxicities can often be medically managed, the latter two may require palliative surgical
528 interventions and extended hospitalization. We show that a single dose of PDP followed by
529 multiple cycles of nal-IRI not only achieved 18-25% tumor-free status in extended survival
530 studies (300-450 days) in two orthotopic PDAC models, but also effectively reduced the
531 endpoint disease burden (both primary tumor weight and the ascites volume). These findings
532 suggest that combination PDP+nal-IRI has the potential to achieve durable improvements in

533 treatment response while significantly improving quality of life in PDAC patients, for whom
534 innovative therapeutic approaches are desperately needed. It is worth mentioning that we
535 demonstrated nal-IRI alone had no statistically significant survival benefit over the 'no-treatment'
536 arm in two human orthotopic models. This is not too surprising, as nal-IRI is, so far, only
537 approved in combination with 5-fluorouracil and leucovorin to treat gemcitabine-refractory
538 metastatic PDAC. Moreover, a slightly lower dose of nal-IRI (20 mg/kg mouse dose; equivalent
539 to ~ 60 mg/m² human dose, a total of 4 cycles) was used in our in vivo study, compared to
540 clinically approved dose (70 mg/m²; an average of ~ 6 cycles). Further research to assess the
541 therapeutic effects of combining PDP with the second-line (nal-IRI + 5-fluorouracil +
542 leucovorin) or front-line (FOLFIRINOX) chemotherapies is warranted.

543 In summary, we suggest that cancers, which are dynamic evolutionary systems exhibiting
544 significant physical barriers to effective drug delivery, may be better managed by PDP combined
545 with chemo or biologic agents. Sub-tumoricidal PDP offers a unique solution to address these
546 obstacles, showing promise for clinical translation to improve therapeutic accessibility and
547 address undesired chemotherapeutic selective pressures for a long-term survival benefit in PDAC
548 models. Given that the feasibility of PDT has already been demonstrated in early PDAC clinical
549 trials(24), leveraging our PDP approach to address the evolutionary challenges associated with
550 standard chemotherapy and increased permeability to enhance the therapeutic index of
551 conventional agents merits further investigations at preclinical and clinical levels.

552

553 **Acknowledgments:** This work was conducted with support from (i) the Photopathology Center
554 of the Wellman Center for Photomedicine, Massachusetts General Hospital, and (ii) the Harvard
555 Catalyst | The Harvard Clinical and Translational Science Center (National Center for Research
556 Resources and the National Center for Advancing Translational Sciences, National Institutes of
557 Health Award UL1 TR001102) and financial contributions from Harvard University and its
558 affiliated academic healthcare centers. The content is solely the responsibility of the authors and
559 does not necessarily represent the official views of Harvard Catalyst, Harvard University and its
560 affiliated academic healthcare centers, or the National Institutes of Health. This work was
561 supported by National Institutes of Health Grants P01CA084203, R01CA156177,
562 R01CA160998 (T.H.), K99CA194269 (H-C.H.), K99CA175292, R00CA175292 (I.R.), and
563 Massachusetts General Hospital Tosteson Fellowship 224889 (H-C.H.). S. Anbil is a Howard
564 Hughes Medical Institute Medical Research Fellow. S. Pereira was supported by the National
565 Institute for Health Research University College London Hospitals Biomedical Research Centre.
566 **Data and materials availability:** Nanoliposomal irinotecan (nal-IRI) was obtained through an
567 MTA.

568

References

- 569
570
571 1. Holohan C, Van Schaeysbroeck S, Longley DB, Johnston PG. Cancer drug resistance: an
572 evolving paradigm. *Nat Rev Cancer* **2013**;13:714-26
573 2. Adiseshiaiah PP, Crist RM, Hook SS, McNeil SE. Nanomedicine strategies to overcome
574 the pathophysiological barriers of pancreatic cancer. *Nature reviews Clinical oncology*
575 **2016**;13:750-65
576 3. Garrido-Laguna I, Hidalgo M. Pancreatic cancer: from state-of-the-art treatments to
577 promising novel therapies. *Nature reviews Clinical oncology* **2015**;12:319-34
578 4. Minchinton AI, Tannock IF. Drug penetration in solid tumours. *Nat Rev Cancer*
579 **2006**;6:583-92
580 5. Greaves M, Maley CC. Clonal evolution in cancer. *Nature* **2012**;481:306-13
581 6. Dy GK, Adjei AA. Understanding, recognizing, and managing toxicities of targeted
582 anticancer therapies. *CA: A Cancer Journal for Clinicians* **2013**;63:249-79
583 7. Wang-Gillam A, Li C-P, Bodoky G, Dean A, Shan Y-S, Jameson G, *et al.*
584 Nanoliposomal irinotecan with fluorouracil and folinic acid in metastatic pancreatic
585 cancer after previous gemcitabine-based therapy (NAPOLI-1): a global, randomised,
586 open-label, phase 3 trial. *The Lancet*;387:545-57
587 8. Bardeesy N, DePinho RA. Pancreatic cancer biology and genetics. *Nat Rev Cancer*
588 **2002**;2:897-909
589 9. Catenacci DV, Junttila MR, Karrison T, Bahary N, Horiba MN, Nattam SR, *et al.*
590 Randomized Phase Ib/II Study of Gemcitabine Plus Placebo or Vismodegib, a Hedgehog
591 Pathway Inhibitor, in Patients With Metastatic Pancreatic Cancer. *Journal of clinical*
592 *oncology : official journal of the American Society of Clinical Oncology* **2015**;33:4284-
593 92
594 10. KJ. L. Stromal uncertainties in pancreatic cancer. *SciBX* **2014**;7
595 11. Rhim Andrew D, Oberstein Paul E, Thomas Dafydd H, Mirek Emily T, Palermo
596 Carmine F, Sastra Stephen A, *et al.* Stromal Elements Act to Restrain, Rather Than
597 Support, Pancreatic Ductal Adenocarcinoma. *Cancer Cell*;25:735-47
598 12. Carnevale J, Ko AH. MM-398 (nanoliposomal irinotecan): emergence of a novel therapy
599 for the treatment of advanced pancreatic cancer. *Future oncology (London, England)*
600 **2016**;12:453-64
601 13. Drummond DC, Noble CO, Guo Z, Hong K, Park JW, Kirpotin DB. Development of a
602 highly active nanoliposomal irinotecan using a novel intraliposomal stabilization strategy.
603 *Cancer Res* **2006**;66:3271-7
604 14. Kalra AV, Kim J, Klinz SG, Paz N, Cain J, Drummond DC, *et al.* Preclinical activity of
605 nanoliposomal irinotecan is governed by tumor deposition and intratumor pro-drug
606 conversion. *Cancer Research* **2014**
607 15. Vives M, Ginestà MM, Gracova K, Graupera M, Casanovas O, Capellà G, *et al.*
608 Metronomic chemotherapy following the maximum tolerated dose is an effective anti-
609 tumour therapy affecting angiogenesis, tumour dissemination and cancer stem cells.
610 *International Journal of Cancer* **2013**;133:2464-72
611 16. Quint K, Tonigold M, Di Fazio P, Montalbano R, Lingelbach S, Ruckert F, *et al.*
612 Pancreatic cancer cells surviving gemcitabine treatment express markers of stem cell
613 differentiation and epithelial-mesenchymal transition. *International journal of oncology*
614 **2012**;41:2093-102

- 615 17. Sergeant G, Vankelecom H, Gremeaux L, Topal B. Role of cancer stem cells in
616 pancreatic ductal adenocarcinoma. *Nature reviews Clinical oncology* **2009**;6:580-6
- 617 18. Guo F, Wang Y, Liu J, Mok SC, Xue F, Zhang W. CXCL12/CXCR4: a symbiotic bridge
618 linking cancer cells and their stromal neighbors in oncogenic communication networks.
619 *Oncogene* **2016**;35:816-26
- 620 19. Li C, Heidt DG, Dalerba P, Burant CF, Zhang L, Adsay V, *et al.* Identification of
621 pancreatic cancer stem cells. *Cancer Res* **2007**;67:1030-7
- 622 20. Arora S, Bhardwaj A, Singh S, Srivastava SK, McClellan S, Nirodi CS, *et al.* An
623 undesired effect of chemotherapy: gemcitabine promotes pancreatic cancer cell
624 invasiveness through reactive oxygen species-dependent, nuclear factor kappaB- and
625 hypoxia-inducible factor 1alpha-mediated up-regulation of CXCR4. *The Journal of*
626 *biological chemistry* **2013**;288:21197-207
- 627 21. Molejon MI, Tellechea JI, Loncle C, Gayet O, Gilabert M, Duconseil P, *et al.*
628 Deciphering the cellular source of tumor relapse identifies CD44 as a major therapeutic
629 target in pancreatic adenocarcinoma. *Oncotarget* **2015**;6:7408-23
- 630 22. Celli JP, Spring BQ, Rizvi I, Evans CL, Samkoe KS, Verma S, *et al.* Imaging and
631 photodynamic therapy: mechanisms, monitoring, and optimization. *Chem Rev*
632 **2010**;110:2795-838
- 633 23. Kessel D, Luo Y, Deng Y, Chang CK. The role of subcellular localization in initiation of
634 apoptosis by photodynamic therapy. *Photochem Photobiol* **1997**;65:422-6
- 635 24. Huggett MT, Jermyn M, Gillams A, Illing R, Mosse S, Novelli M, *et al.* Phase I/II study
636 of verteporfin photodynamic therapy in locally advanced pancreatic cancer. *Br J Cancer*
637 **2014**;110:1698-704
- 638 25. Huang HC, Mallidi S, Liu J, Chiang CT, Mai Z, Goldschmidt R, *et al.* Photodynamic
639 Therapy Synergizes with Irinotecan to Overcome Compensatory Mechanisms and
640 Improve Treatment Outcomes in Pancreatic Cancer. *Cancer Res* **2016**;76:1066-77
- 641 26. Spring BQ, Bryan Sears R, Zheng LZ, Mai Z, Watanabe R, Sherwood ME, *et al.* A
642 photoactivable multi-inhibitor nanoliposome for tumour control and simultaneous
643 inhibition of treatment escape pathways. *Nature nanotechnology* **2016**;11:378-87
- 644 27. Kawato Y, Aonuma M, Hirota Y, Kuga H, Sato K. Intracellular roles of SN-38, a
645 metabolite of the camptothecin derivative CPT-11, in the antitumor effect of CPT-11.
646 *Cancer Res* **1991**;51:4187-91
- 647 28. Chen B, Pogue BW, Hoopes PJ, Hasan T. Combining vascular and cellular targeting
648 regimens enhances the efficacy of photodynamic therapy. *Int J Radiat Oncol Biol Phys*
649 **2005**;61:1216-26
- 650 29. Torchilin VP. Recent advances with liposomes as pharmaceutical carriers. *Nature*
651 *reviews Drug discovery* **2005**;4:145-60
- 652 30. Ko AH, Tempero MA, Shan YS, Su WC, Lin YL, Dito E, *et al.* A multinational phase 2
653 study of nanoliposomal irinotecan sucrosfate (PEP02, MM-398) for patients with
654 gemcitabine-refractory metastatic pancreatic cancer. *British Journal of Cancer*
655 **2013**;109:920-5
- 656 31. H.C. H, T. H. The “Nano” World in Photodynamic Therapy *Austin J Nanomed*
657 *Nanotechnol* **2014**;2:1020
- 658 32. Willyard C. Cancer therapy: an evolved approach. *Nature* **2016**;532:166-8
- 659 33. Makohon-Moore A, Iacobuzio-Donahue CA. Pancreatic cancer biology and genetics
660 from an evolutionary perspective. *Nat Rev Cancer* **2016**;16:553-65

- 661 34. Gradiz R, Silva HC, Carvalho L, Botelho MF, Mota-Pinto A. MIA PaCa-2 and PANC-1
662 – pancreas ductal adenocarcinoma cell lines with neuroendocrine differentiation and
663 somatostatin receptors. *Scientific Reports* **2016**;6:21648
- 664 35. Wei HJ, Yin T, Zhu Z, Shi PF, Tian Y, Wang CY. Expression of CD44, CD24 and ESA
665 in pancreatic adenocarcinoma cell lines varies with local microenvironment.
666 *Hepatobiliary & pancreatic diseases international : HYPD INT* **2011**;10:428-34
- 667 36. Deer EL, Gonzalez-Hernandez J, Coursen JD, Shea JE, Ngatia J, Scaife CL, *et al.*
668 Phenotype and genotype of pancreatic cancer cell lines. *Pancreas* **2010**;39:425-35
- 669 37. Wu YM, Nowack DD, Omenn GS, Haab BB. Mucin glycosylation is altered by pro-
670 inflammatory signaling in pancreatic-cancer cells. *Journal of proteome research*
671 **2009**;8:1876-86
- 672 38. Awasthi N, Zhang C, Schwarz AM, Hinz S, Wang C, Williams NS, *et al.* Comparative
673 benefits of Nab-paclitaxel over gemcitabine or polysorbate-based docetaxel in
674 experimental pancreatic cancer. *Carcinogenesis* **2013**;34:2361-9
- 675 39. Fidler IJ, Ellis LM. Chemotherapeutic drugs--more really is not better. *Nature medicine*
676 **2000**;6:500-2
- 677 40. Hanahan D, Bergers G, Bergsland E. Less is more, regularly: metronomic dosing of
678 cytotoxic drugs can target tumor angiogenesis in mice. *The Journal of clinical*
679 *investigation* **2000**;105:1045-7
- 680 41. Browder T, Butterfield CE, Kraling BM, Shi B, Marshall B, O'Reilly MS, *et al.*
681 Antiangiogenic scheduling of chemotherapy improves efficacy against experimental
682 drug-resistant cancer. *Cancer Res* **2000**;60:1878-86
- 683 42. Klement G, Baruchel S, Rak J, Man S, Clark K, Hicklin DJ, *et al.* Continuous low-dose
684 therapy with vinblastine and VEGF receptor-2 antibody induces sustained tumor
685 regression without overt toxicity. *The Journal of clinical investigation* **2000**;105:R15-24
- 686 43. Gatenby RA, Silva AS, Gillies RJ, Frieden BR. Adaptive Therapy. *Cancer Research*
687 **2009**;69:4894-903
- 688 44. Gatenby RA, Brown J, Vincent T. Lessons from applied ecology: cancer control using an
689 evolutionary double bind. *Cancer Res* **2009**;69:7499-502
- 690 45. Iacobuzio-Donahue CA, Fu B, Yachida S, Luo M, Abe H, Henderson CM, *et al.* DPC4
691 gene status of the primary carcinoma correlates with patterns of failure in patients with
692 pancreatic cancer. *Journal of clinical oncology : official journal of the American Society*
693 *of Clinical Oncology* **2009**;27:1806-13
- 694 46. Castano AP, Mroz P, Hamblin MR. Photodynamic therapy and anti-tumour immunity.
695 *Nat Rev Cancer* **2006**;6:535-45
- 696 47. Siegel RL, Miller KD, Jemal A. Cancer statistics, 2016. *CA Cancer J Clin* **2016**;66:7-30
- 697 48. Buanes TA. Pancreatic cancer-improved care achievable. *World Journal of*
698 *Gastroenterology : WJG* **2014**;20:10405-18
- 699 49. Gourgou-Bourgade S, Bascoul-Mollevis C, Desseigne F, Ychou M, Bouche O, Guimbaud
700 R, *et al.* Impact of FOLFIRINOX compared with gemcitabine on quality of life in
701 patients with metastatic pancreatic cancer: results from the PRODIGE 4/ACCORD 11
702 randomized trial. *Journal of clinical oncology : official journal of the American Society*
703 *of Clinical Oncology* **2013**;31:23-9
- 704 50. Saif MW, Siddiqui IAP, Sohail MA. Management of ascites due to gastrointestinal
705 malignancy. *Annals of Saudi Medicine* **2009**;29:369-77
- 706

707 **Figure Legends:**

708 **Fig.1.** *Concept of sub-tumoricidal photodynamic priming.* Spatiotemporally controlled
709 photodynamic priming (PDP) of tumor microvasculature and parenchyma simultaneously
710 improves therapeutic agent accessibility and overcomes chemotherapeutic selection
711 pressures. Subtumoricidal PDP increases tumor permeability to enhance intratumoral
712 accumulation of chemotherapeutic agents for a prolonged period of time. In addition, it
713 attenuates the insidious surge of stemness marker expression that is typically observed
714 after multiple cycles of chemotherapy. Combining subtumoricidal PDP with cytotoxic
715 chemotherapeutic agents prevents aggressive tumor regrowth, reduces metastatic burden,
716 and enhances survival outcomes.

717 **Fig.2.** *PDP increases tumor vascular permeability to enhance nal-IRI delivery in an orthotopic*
718 *PDAC model.* Orthotopic MIA PaCa-2 tumors were exposed to 75 J/cm² of light (100
719 mW/cm²) one-hour following intravenous injection of nal-BPD (0.25 mg/kg) and a single
720 dose of Dil5-nal-IRI (20 mg/kg). Control tumors were only injected with Dil5-nal-IRI (20
721 mg/kg) without light treatment. (A) Representative confocal fluorescence microscopy
722 images of control tumors (top row) and PDP-treated tumors (bottom row) obtained 4
723 hours after intravenous injection Dil5-nal-IRI. In presence of PDP, Dil5-nal-IRI (red) was
724 widely distributed throughout the tumor tissue and extravasated from the blood vessels
725 (tomato lectin staining; green), whereas the signals arising from Dil5-nal-IRI in control
726 tumors were confined to the immediate vicinity of the tumor blood vessels. No Dil5-nal-
727 IRI signal was detected in the tumors treated with PDP alone. Nuclear staining (blue-
728 fluorescence, DAPI); Scale bar 200 μm. (B, C) Quantitative analyses of Dil5-nal-IRI
729 fluorescence intensity (B) and distribution (C) showing PDP significantly enhanced Dil5-

730 nal-IRI accumulation and extravasation within MIA PaCa-2 tumors 4 and 24 hours after
731 Dil5-nal-IRI injection ($n \geq 3$ animals per group; $n \geq 19$ images per group; $***P < 0.001$,
732 Bonferroni-corrected Mann-Whitney U test). (D, E) PDP mediated changes in tumor
733 pharmacokinetic profile of nal-IRI. Swiss nude mice bearing orthotopic MIA PaCa-2
734 tumors were treated with a single cycle of nal-IRI (nal-IRI, 20 mg/kg; IV) (red line; solid
735 square) or a combination of PDP and single cycle nal-IRI (20 mg/kg; IV) (blue line; solid
736 circle). Tumors were collected at various intervals and the irinotecan (d) and SN-38 (e)
737 levels were measured by HPLC analysis ($n \geq 5$ per time point; $***P < 0.01$, $**P = 0.022$,
738 $*P < 0.05$, Bonferroni-corrected Mann-Whitney U test). (F) Carboxylesterase (CES)
739 activities in MIA PaCa-2 tumors were not modulated by PDP at various time posts after
740 treatment ($n = 3-9$ animals *per* condition; *ns*, non-significant, Kruskal–Wallis one-way
741 ANOVA). (G) Comparison of tumoral irinotecan to SN-38 molar ratio at various time-
742 points between ‘single cycle nal-IRI’ monotherapy and ‘PDP + single cycle nal-IRI’ arm.
743 ($n \geq 5$ per time point; *Solid lines* are nonlinear fits; *n.s.*, non-significant, $P = 0.79$, two-way
744 ANOVA PDP·time interaction term). Results are mean \pm standard error of the mean
745 (SEM).

746 **Fig.3.** PDP of tumors extends the efficacy of multi-cycle nal-IRI chemotherapy for durable
747 tumor control in two orthotopic PDAC models. (A) *In vivo* treatment schedule:
748 Treatments were initiated nine days after MIA PaCa-2 or AsPC-1 cancer cell
749 implantation when tumor volumes reached approximately 50 mm^3 (see Methods). Mice
750 were randomized into groups that received (i) no-treatment, (ii) PDP (nal-BPD 0.25
751 mg/kg; 690 nm light at 100 mW/cm^2 to achieve 75 J/cm^2), (iii) nal-IRI (four doses, each
752 at 20 mg/kg irinotecan hydrochloride salt, on days 9, 12, 17, and 21 after tumor

753 implantation), and (iv) combination of PDP and nal-IRI (PDP+nal-IRI). Injections of nal-
754 BPD (for PDP) and nal-IRI were done intravenously. **(B-E)** Orthotopic MIA PaCa-2 and
755 **(F-I)** AsPC-1 tumor volumes were longitudinally monitored by non-invasive ultrasound
756 imaging. A combination of PDP and nal-IRI prolonged and enhanced tumor growth
757 inhibition in both MIA PaCa-2 and AsPC-1 animal models compared to nal-IRI alone. (n
758 = 9-13 for MIA PaCa-2 model; n = 5-7 for AsPC-1 model; $*P<0.05$, $***P<0.001$, one-
759 way ANOVA with Tukey's post hoc test for 'nal-IRI' vs. 'PDP+nal-IRI' groups). **(C, G)**
760 Gross tumor volume changes were quantified between day 8 (one day prior to treatment)
761 and approximately day 30 (21 days after treatment initiation) in **(C)** MIA PaCa-2 and **(G)**
762 AsPC-1 orthotopic xenograft models. Approximately, a 90% reduction in mean tumor
763 volume was observed in mice treated with 'nal-IRI' and 'PDP+nal-IRI' compared to the
764 'no-treatment' control animals. Asterisks denote significance compared with no-
765 treatment group or amongst the indicated groups at each time point. ($*P<0.05$, $**P<0.01$,
766 $***P<0.001$, *n.s.*, non-significant, Kruskal–Wallis one-way ANOVA with Dunn's post
767 hoc test) The specific growth rate (SGR) of tumors during the *treatment period* **(D, H)**
768 and *post-treatment period* **(E, I)** were determined using the following formula: $SGR =$
769 $(1/V)(dV/dt)$, where V is tumor volume and t is time. In the MIA PaCa-2 mouse model,
770 shortly following the termination of treatment and up to 120 days, nal-IRI-treated animals
771 experienced a rapid tumor regrowth at a significantly higher SGR (4.8 ± 0.3 %/d),
772 compared to the 'no-treatment' control tumors. In contrast, the combination of PDP and
773 nal-IRI continued to suppress tumor growth to a low SGR (1.7 ± 0.9 %/d) for a prolonged
774 period of time up to 120 days. ($*P<0.05$, $**P<0.01$, $***P<0.001$, *n.s.*, non-significant,
775 Kruskal–Wallis one-way ANOVA with Dunn's post hoc test). (n = 9-13 mice per group

776 for MIA PaCa-2 model; $n = 5-7$ for AsPC-1 model). Results are mean \pm standard error of
777 the mean (SEM).

778 **Fig.4.** *PDP suppresses chemotherapy-induced enrichment of CD44 and CXCR4 expression in*
779 *PDAC tumors. (A)* Representative immunofluorescence images of CD44 and CXCR4 in
780 MIA PaCa-2 tumors subjected to (1) no-treatment; (2) PDP (nal-BPD 0.25 mg/kg; 690
781 nm light at 100 mW/cm² to achieve 75 J/cm²); (3) four cycles of nal-IRI (nal-IRI; at 20
782 mg/kg each, on days 9, 12, 17 and 21); and (4) PDP+nal-IRI. Significant increases in
783 CD44 and CXCR4 expression were observed in tumors treated with nal-IRI alone at days
784 60 and 120 post-implantation; Blue: DAPI (nuclei), Red: CD44, Green: CXCR4. Scale
785 bar, 100 μ m. **(B, C)** To quantify immunofluorescence intensities, at least 25 images,
786 evenly distributed across the entire tumor cross-section, were collected from at least three
787 tumor samples for each condition. CD44 and CXCR4 fluorescence intensities were
788 normalized to DAPI area per image. Relative CD44 and CXCR4 levels were found to be
789 significantly higher in the ‘nal-IRI’ groups compared to other groups. (* $P < 0.05$,
790 ** $P < 0.01$, *** $P < 0.001$, Kruskal–Wallis one-way ANOVA with Dunn’s post hoc test)
791 Asterisks denote significance compared to the no-treatment group or amongst the
792 indicated groups at each time point. **(D, E)** Representative immunoblotting of CD44 and
793 CXCR4 in tumors collected at day 120 confirmed that the enhanced protein expression of
794 CD44 and CXCR4 after nal-IRI treatment could be effectively mitigated by PDP. **(F)**
795 Representative CD44/CXCR4 double-stained images of MIA PaCa-2 tumors subjected to
796 (1) no-treatment; (2) PDP (nal-BPD 0.25 mg/kg; 690 nm light at 100 mW/cm² to achieve
797 75 J/cm²); (3) four cycles of nal-IRI (nal-IRI; at 20 mg/kg each, on days 9, 12, 17 and
798 21); and (4) PDP+nal-IRI. **(G)** The CD44+, CXCR4+, and CD44+/CXCR4+ areas of

799 tumors (collected at day 120) were quantified and normalized to DAPI area using ImageJ
800 software. At least 12 images, evenly distributed across the entire tumor cross-section,
801 were collected from at least four tumor samples for each condition. (* $P < 0.05$, ** $P < 0.01$,
802 *** $P < 0.001$, Kruskal–Wallis one-way ANOVA with Dunn’s post hoc test) Asterisks
803 denote significance compared to the no-treatment group or amongst the indicated groups
804 at each time point. **(H)** Immunoblot analysis of E-cadherin in MIA PaCa-2 primary tumor
805 tissues at days 60 and 120. Expression of E-cadherin (relative to ‘PDP+nal-IRI’ at day
806 120) was normalized to glyceraldehyde 3-phosphate dehydrogenase (GAPDH) ($n = 2-3$;
807 * $P < 0.05$, ** $P < 0.01$, *** $P < 0.001$, One-way ANOVA with Tukey’s post hoc test). **(I)**
808 Representative Immunoblotting showed that the no-treatment, PDP, nal-IRI and treated
809 tumors exhibited a complete loss of E-Cadherin expression, suggesting that ‘PDP+nal-
810 IRI’ may help reduce the dedifferentiation of cancer cells. Results in B, C, D, E and I are
811 mean \pm standard error of the mean (SEM).

812 **Fig.5.** *PDP enhances the anti-metastatic effects of multi-cycle nal-IRI in vivo.* **(A)** To assess the
813 efficacy of PDP and nal-IRI in controlling metastases, treatments were initiated nine days
814 after MIA PaCa-2 tumor implantation in mice randomized to the following groups: (i)
815 no-treatment; (ii) PDP (nal-BPD 0.25 mg/kg; 690 nm light at 100 mW/cm² to achieve 75
816 J/cm²); (iii) nal-IRI (four doses at 20 mg/kg each, on days 9, 12, 17 and 21); and (iv)
817 PDP+nal-IRI. **(B-D)** The number of metastases to the liver, retroperitoneal lymph nodes,
818 diaphragm and lung were quantified by qRT-PCR (see Methods) on day 60 and day 120
819 after tumor implantation. ($n > 11$ per group; * $P < 0.05$, ** $P < 0.01$, *** $P < 0.001$, Kruskal–
820 Wallis one-way ANOVA with Dunn’s post hoc test). Asterisks denote significance
821 compared with no-treatment group or amongst the indicated groups at each time point.

822 (B, C) The overall metastatic burden includes liver, lung, retroperitoneal lymph nodes,
823 and diaphragm metastases. (D) Metastases to individual organs are presented. At day 60,
824 both 'nal-IRI' and 'PDP+nal-IRI' completely inhibited liver metastasis and significantly
825 reduced distant organ metastases to less than 50 cancer cells, as compared to the 'no-
826 treatment' group (>1 million cancer cells at lung, diaphragm, lymph node). At day 120,
827 the combination treatment of PDP and nal-IRI significantly reduced liver and distant
828 organ metastases by ~16,000-fold and ~40,000-fold ($P<0.001$), respectively, compared to
829 the 'no-treatment' control. (E) The incidence of metastases in mice bearing orthotopic
830 MIA PaCa-2 tumors were significantly reduced by the combination treatment on days 60
831 and 120 ($n > 11$ per group). At day 120, the combination of PDP and nal-IRI effectively
832 reduced the incidence of metastases to a range from 6.7 to 33.3%, while the incidence of
833 metastases ranged from 60 to 100% in the 'no-treatment', 'PDP', and 'nal-IRI' groups.

834 **Fig.6.** PDP and multi-cycle nal-IRI achieve durable and significant survival enhancement and
835 reduce endpoint disease burden in two orthotopic PDAC models. (A) Swiss nude mice
836 were orthotopically inoculated with MIA PaCa-2 or AsPC-1 cells, divided into four
837 groups, and subjected to (1) no-treatment; (2) PDP (day 9 post-implantation; nal-BPD
838 0.25 mg/kg; 690 nm light at 100 mW/cm² to achieve 75 J/cm²); (3) multiple cycles of
839 nal-IRI (nal-IRI; four doses at 20 mg/kg each, on days 9, 12, 17 and 21 post-
840 implantation); and (4) PDP+nal-IRI. Moribundity was used as the endpoint for the
841 survival study with proper justification and special approval by the MGH IACUC.
842 Animals were monitored for up to 450 days (15 months). (B, C) Kaplan-Meier plot of
843 overall animal survival (B) and progression-free survival (C) in MIA PACa-2 model. (n
844 = 9-13 animals per group). (D) Kaplan-Meier plot of animal overall survival in the

845 AsPC-1 model. ($n = 4-7$ animals per group). (E) Median survival time, hazard ratio forest
846 plot, and differences in survival were evaluated by the log-rank test. A global test
847 demonstrated a difference exists among the groups. Specifically, pairwise comparisons
848 were performed to evaluate the advantage of treatment over no-treatment. Animals
849 treated with PDP+nal-IRI were found to be significantly less likely to die by the next
850 time point (hazard ratio < 1). No advantage to monotherapies (compared to no-treatment)
851 were observed. Primary tumor weight, metastatic burden, and ascites volume were
852 evaluated at animal death or day 450. (F) The combination of PDP+nal-IRI
853 significantly reduced the endpoint primary tumor weight by half compared to the
854 monotherapies and the no-treatment group. ($n = 3-5$ animals per group, $*P < 0.05$,
855 Unpaired t test). (G) The ascites formation in moribund animals were significantly
856 reduced after 'nal-IRI' and 'PDP+nal-IRI' treatments, compared to the 'no-treatment'
857 arm. ($n = 3-6$ animals *per* group; ($*P < 0.05$, $**P < 0.01$, Unpaired t test). Asterisks denote
858 significance compared with no-treatment group or amongst the indicated groups at each
859 time point. Results are mean \pm standard error of the mean (SEM).

Figure 1

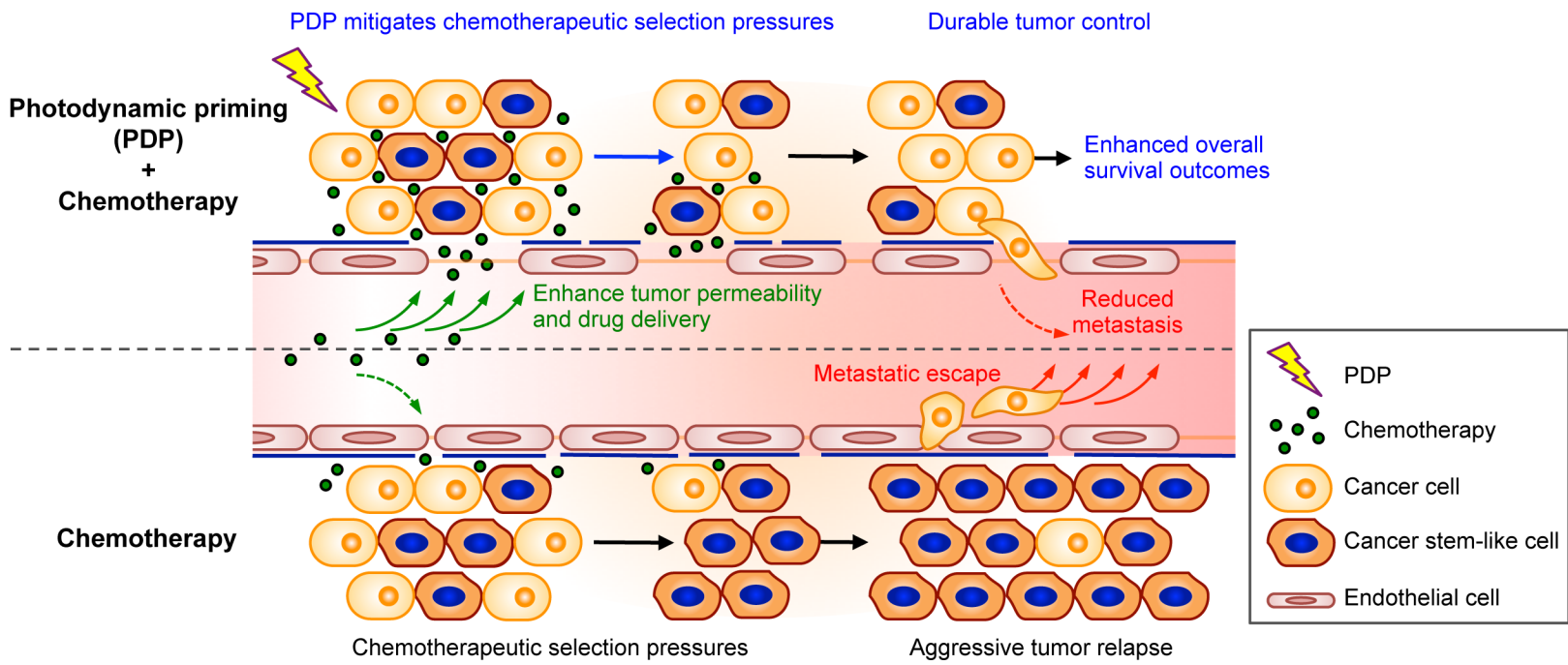


Figure 2

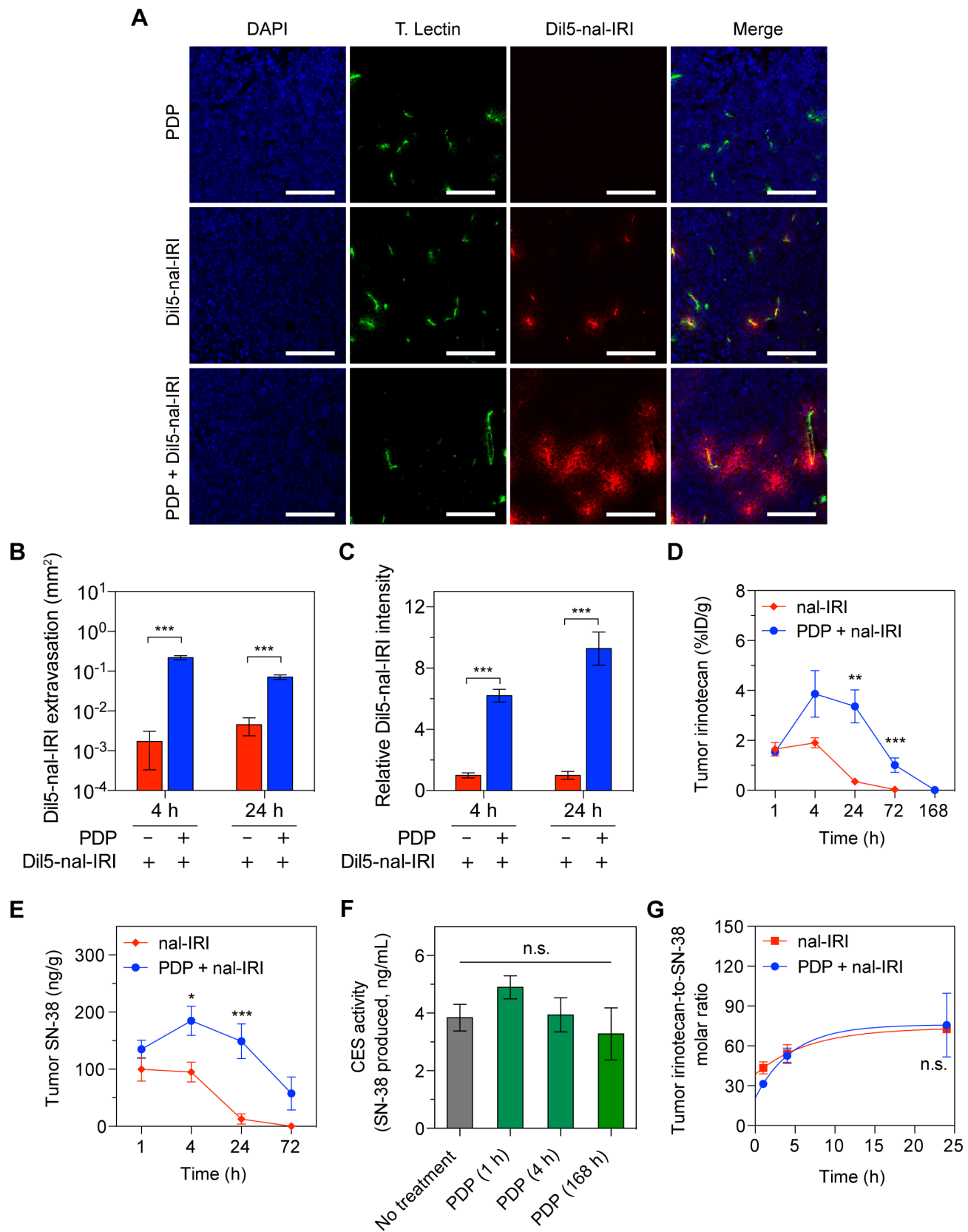


Figure 3

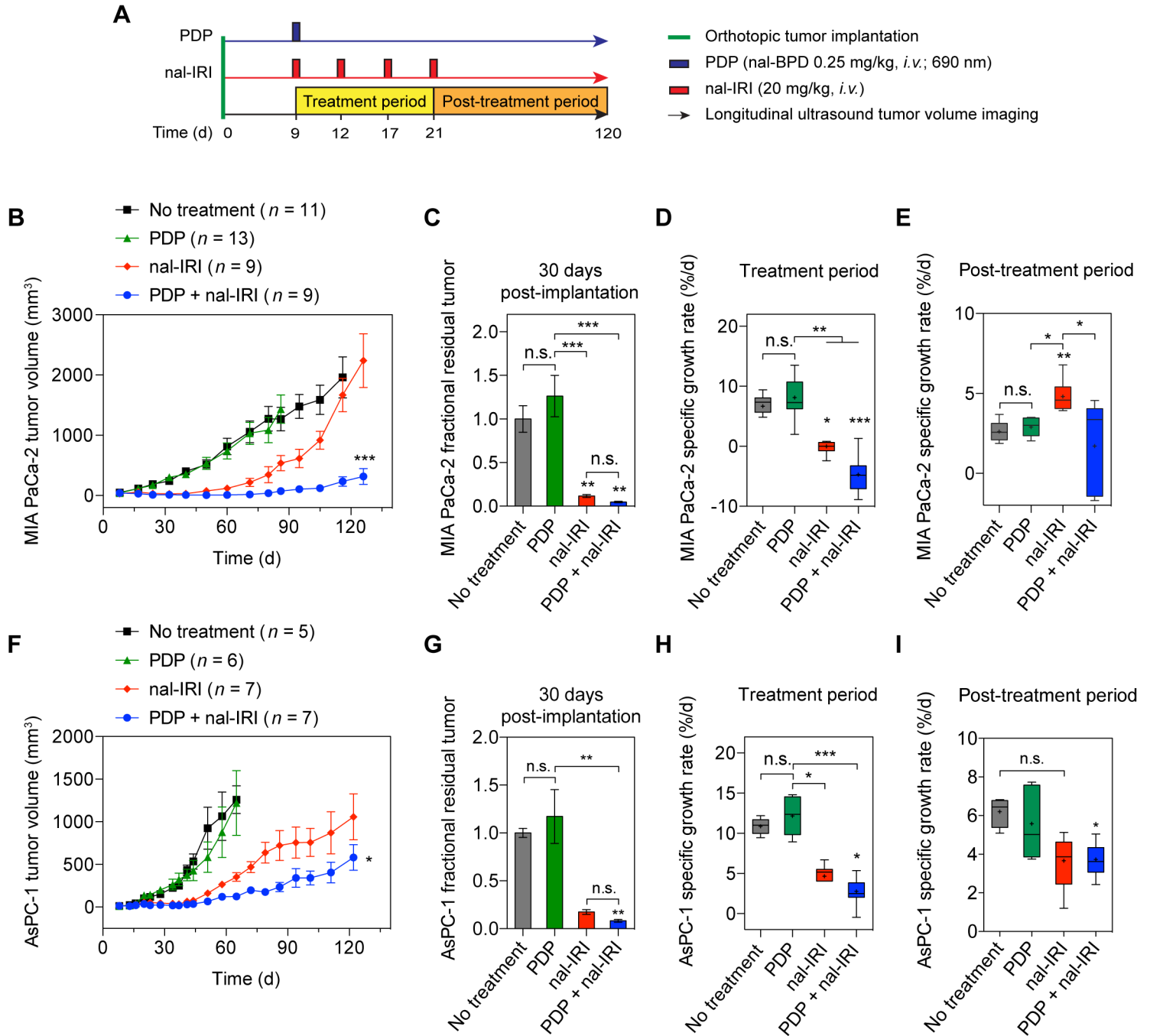


Figure 4

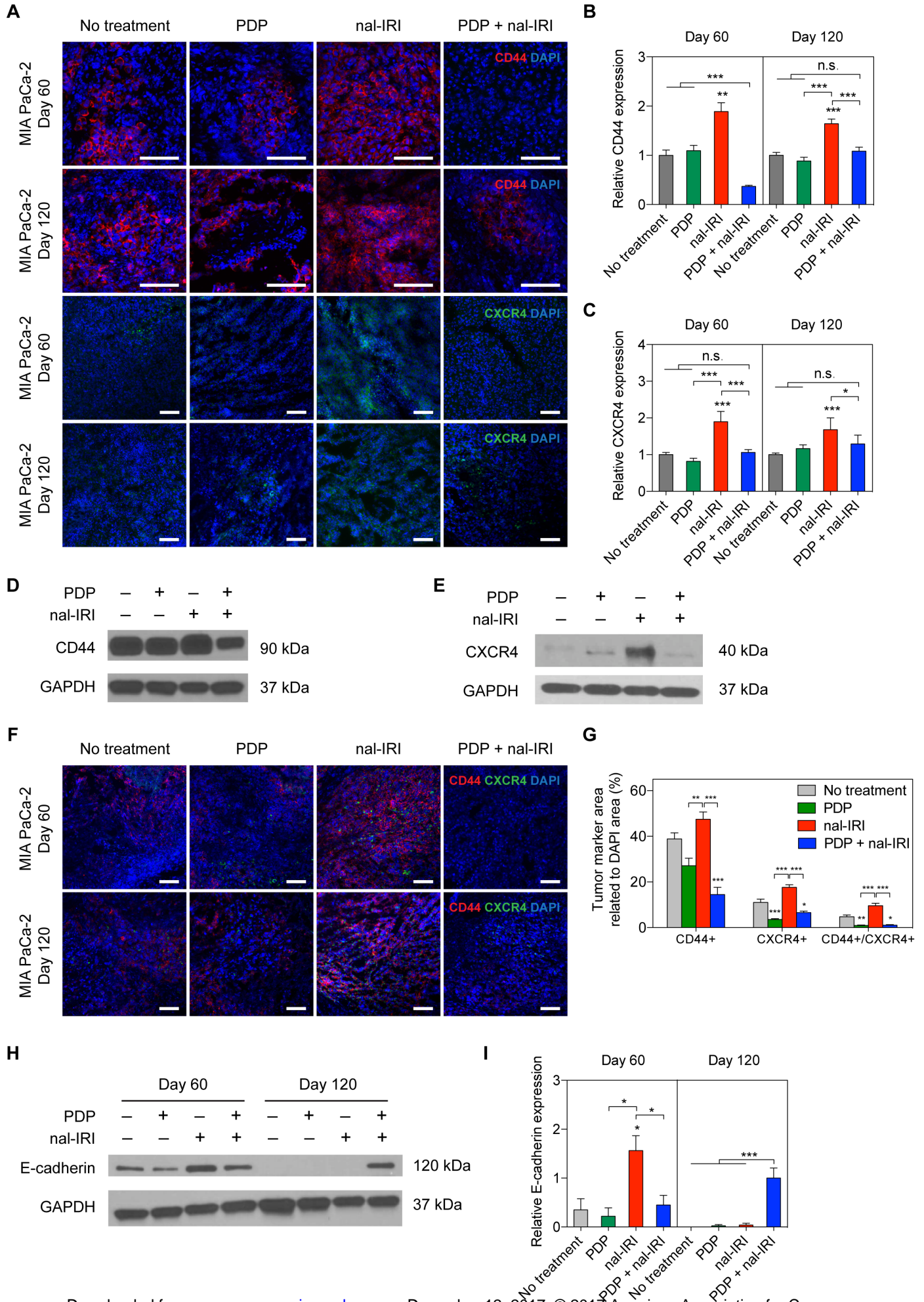
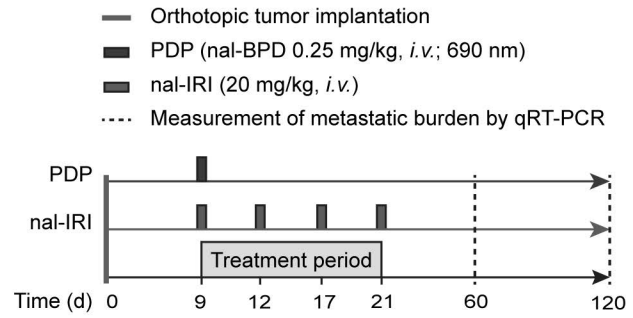
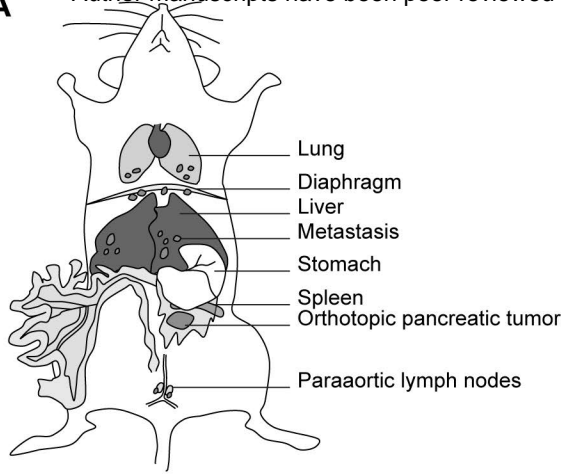


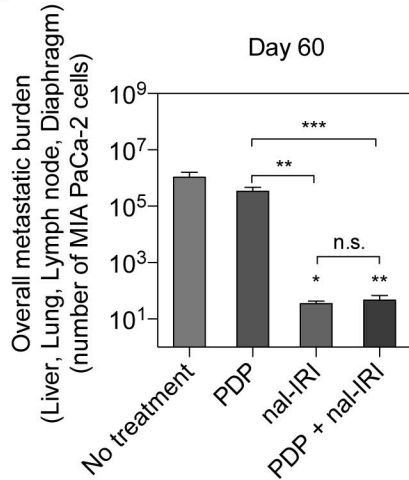
Figure 5

Author Manuscript Published OnlineFirst on November 29, 2017; DOI: 10.1158/0008-5472.CAN-17-1700
 Author manuscripts have been peer reviewed and accepted for publication but have not yet been edited.

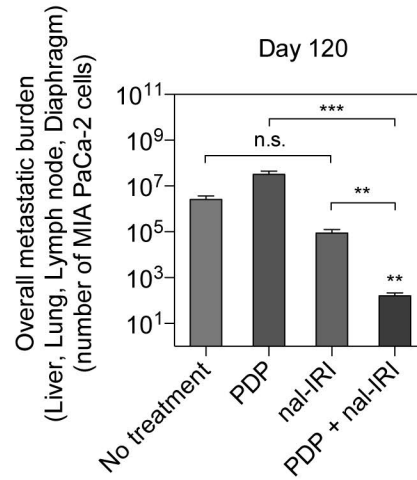
A



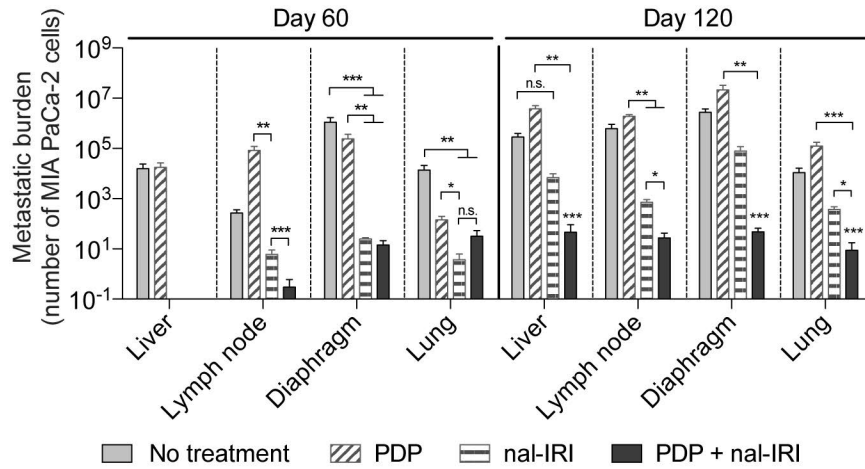
B



C



D



E

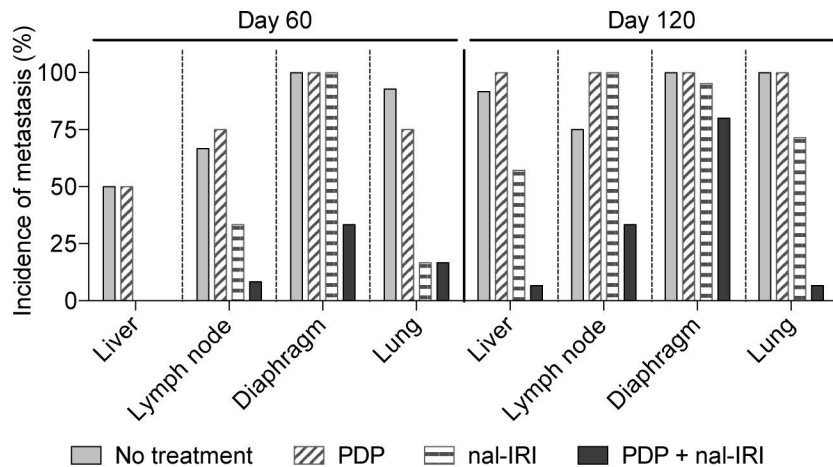
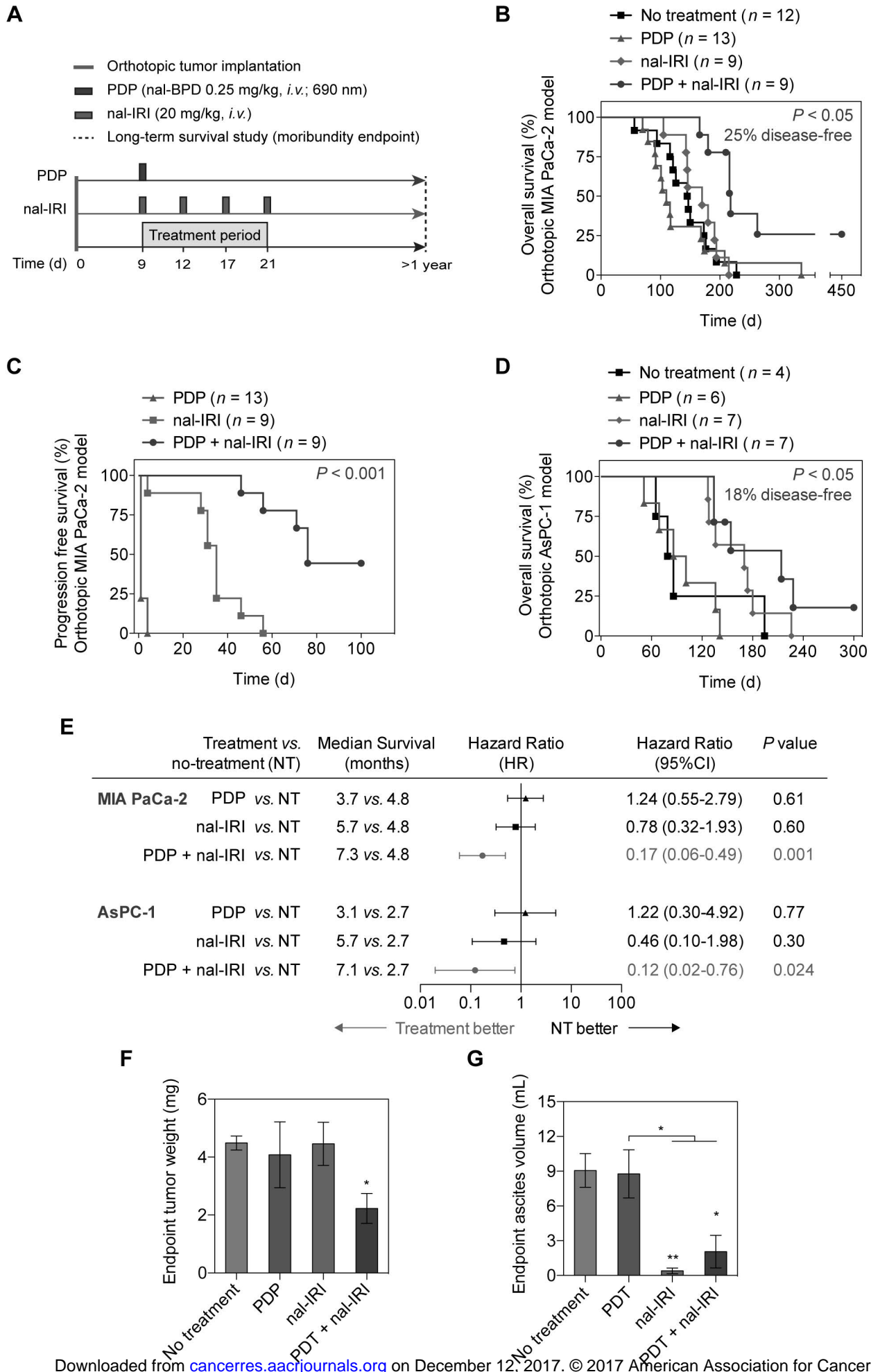


Figure 6



Cancer Research

The Journal of Cancer Research (1916–1930) | The American Journal of Cancer (1931–1940)

Photodynamic priming mitigates chemotherapeutic selection pressures and improves drug delivery

Huang-Chiao Huang, Imran Rizvi, Joyce Liu, et al.

Cancer Res Published OnlineFirst November 29, 2017.

Updated version	Access the most recent version of this article at: doi: 10.1158/0008-5472.CAN-17-1700
Supplementary Material	Access the most recent supplemental material at: http://cancerres.aacrjournals.org/content/suppl/2017/11/29/0008-5472.CAN-17-1700.DC1
Author Manuscript	Author manuscripts have been peer reviewed and accepted for publication but have not yet been edited.

E-mail alerts [Sign up to receive free email-alerts](#) related to this article or journal.

Reprints and Subscriptions To order reprints of this article or to subscribe to the journal, contact the AACR Publications Department at pubs@aacr.org.

Permissions To request permission to re-use all or part of this article, use this link <http://cancerres.aacrjournals.org/content/early/2017/11/29/0008-5472.CAN-17-1700>. Click on "Request Permissions" which will take you to the Copyright Clearance Center's (CCC) Rightslink site.